SANDIA REPORT
SAND2012-0530
Unlimited Release
Printed June 2011

Assessment of Existing Sierra/Fuego Capabilities Related to Grid-To-Rod-Fretting (GTRF)

Salvador B. Rodriguez and Daniel Z. Turner

Prepared by
Sandia National Laboratories
Albuquerque, New Mexico 87185 and Livermore, California 94550

Sandia National Laboratories is a multi-program laboratory managed and operated by Sandia Corporation, a wholly owned subsidiary of Lockheed Martin Corporation, for the U.S. Department of Energy's National Nuclear Security Administration under contract DE-AC04-94AL85000.

Approved for public release; further dissemination unlimited.

Issued by Sandia National Laboratories, operated for the United States Department of Energy by Sandia Corporation.

NOTICE: This report was prepared as an account of work sponsored by an agency of the United States Government. Neither the United States Government, nor any agency thereof, nor any of their employees, nor any of their contractors, subcontractors, or their employees, make any warranty, express or implied, or assume any legal liability or responsibility for the accuracy, completeness, or usefulness of any information, apparatus, product, or process disclosed, or represent that its use would not infringe privately owned rights. Reference herein to any specific commercial product, process, or service by trade name, trademark, manufacturer, or otherwise, does not necessarily constitute or imply its endorsement, recommendation, or favoring by the United States Government, any agency thereof, or any of their contractors or subcontractors. The views and opinions expressed herein do not necessarily state or reflect those of the United States Government, any agency thereof, or any of their contractors.

Printed in the United States of America. This report has been reproduced directly from the best available copy.

Available to DOE and DOE contractors from
U.S. Department of Energy
Office of Scientific and Technical Information
P.O. Box 62
Oak Ridge, TN 37831

Telephone: (865) 576-8401
Facsimile: (865) 576-5728
E-Mail: reports@adonis.osti.gov
Online ordering: http://www.osti.gov/bridge

Available to the public from
U.S. Department of Commerce
National Technical Information Service
5285 Port Royal Rd
Springfield, VA 22161

Telephone: (800) 553-6847
Facsimile: (703) 605-6900
E-Mail: orders@ntis.fedworld.gov
Online ordering: http://www.ntis.gov/help/ordermethods.asp?loc=7-4-0#online

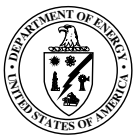

SAND2012-0530
Unlimited Release
Printed June 2011

Assessment of Existing Sierra/Fuego Capabilities Related to Grid-To-Rod-Fretting (GTRF)

Salvador B. Rodriguez and Daniel Z. Turner

Fire and Aerosol Sciences
Sandia National Laboratories
P.O. Box 5800
Albuquerque, New Mexico 87185-0825

Abstract

The following report presents an assessment of existing capabilities in Sierra/Fuego applied to modeling several aspects of grid-to-rod-fretting (GTRF) including: fluid dynamics, heat transfer, and fluid-structure interaction. We compare the results of a number of Fuego simulations with relevant sources in the literature to evaluate the accuracy, efficiency, and robustness of using Fuego to model the aforementioned aspects. Comparisons between flow domains that include the full fuel rod length vs. a subsection of the domain near the spacer show that tremendous efficiency gains can be obtained by truncating the domain without loss of accuracy. Thermal analysis reveals the extent to which heat transfer from the fuel rods to the coolant is improved by the swirling flow created by the mixing vanes. Lastly, coupled fluid-structure interaction analysis shows that the vibrational modes of the fuel rods filter out high frequency turbulent pressure fluctuations. In general, these results allude to interesting phenomena for which further investigation could be quite fruitful.

Contents

Introduction

Fuego is a 3D, incompressible, reactive flow, massively parallel, generalized unstructured, computational fluid dynamics (CFD) code with state-of-the-art turbulence models as well as laminar and buoyant flow capabilities [1]. It includes Reynolds-averaged Navier-Stokes (RANS) and large eddy simulation (LES) models. The RANS models include v2-f, low Re k-ϵ, standard k-ϵ, as well as many others. Among Fuego's more sophisticated LES models are the KSGS, Smagorinsky, and dynamic Smagorinsky models. For anisotropic turbulent flow fields with complex mixing and swirling (similar to those found in nuclear reactor fuel assemblies) the dynamic Smagorinsky turbulence model compares excellently with experimental data (for examples see [2, 3, 4]) and will be the model of choice for this work. In addition, the code has a wide variety of flux limiters and combustion models, as well as participating media radiation (PMR) and conjugate heat transfer (CHT) capabilities. Fuego also includes Lagrangian transport capabilities appropriate for modeling particles and drops, some deposition modeling physics, and basic chemistry models. The code is currently being developed at Sandia National Laboratories (SNL) as part of a set of strategic, comprehensive codes funded through the Advanced Simulation and Computing (ASC) program.

Fuego handles the convective operator in a *hybrid* fashion with varying degrees of upwind and centered approaches. Here, *hybrid* refers to the blending between the upwind and centered schemes. Upwinding works by dampening the over- and under-shoots of spurious oscillations, but produces excessive diffusion. As a consequence, secondary vortices generally do not develop during reactive flow simulations. Excessive diffusion in reactive flow simulations leads to the formation of non-physical, large, lumped bulbous structures that resemble mushroom heads. Thus, a first order upwind method can smooth out oscillations, but may do so at the expense of an overly-dissipated solution.

Recently, Fuego has undergone extensive validation and verification (V&V) testing on flows that include: conventional jets, swirling jets, jets in crossflow, swirling jets in crossflow, flows around a vertical cylinder, staggered tubes in crossflows, and mixed convection heat transfer to heated horizontal cylinders in crossflow. A summary of these results in included in the appendix.

Model Description

Regarding damage to reactor components caused by vibrations, of primary interest is the vibrational excitation of the fuel rods induced by fluctuations in the flow of coolant through the reactor. To capture this influence we define a model that represents a simplified section of the fuel rod array that can be used to study the relevant excitation mechanisms.

Problem geometry

Figure 1 shows the layout and dimensions of the CFD model, which corresponds to the Westinghouse V5H fuel assembly [5]. A portion of the domain has been removed to show the spacer and the fuel rod at the center. The length of the model is consistent with one fuel rod span from mixing vane to mixing vane. The model is offset by half of the span length such that a single mixing vane lies at the center of the model.

In some cases a shorter domain is used. The short domain (denoted *3d-10d*) is identical to the domain in Figure 1 (denoted *full*), with the exception that the inflow boundary is three rod diameters upstream of the spacer and the outflow boundary is ten diameters downstream.

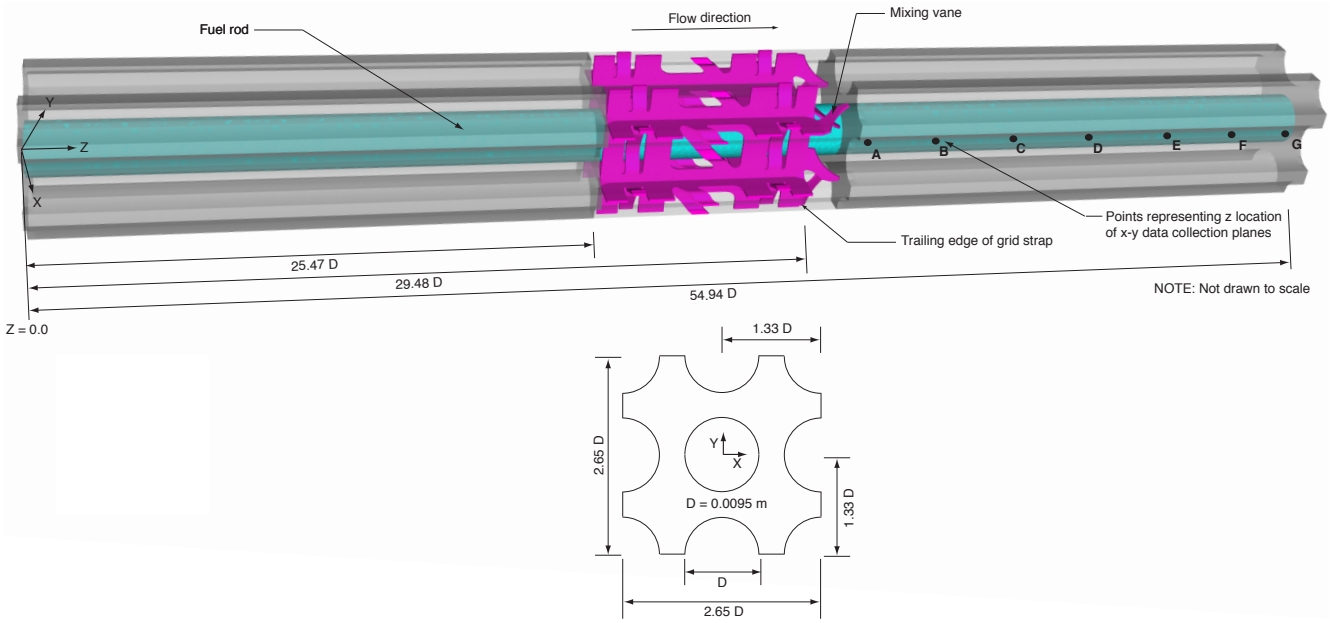

Figure 1: Problem geometry and dimensions. The middle section of the domain has been removed to show the spacer.

Boundary conditions

The boundary conditions for this problem are shown in Figure 2. The inflow boundary condition consists of a uniform inlet velocity of 5.0 m/s. At the outflow boundary, an open boundary condition is used for which the pressure is specified as $p^{spec} = 0.0\ Pa$. On the outflow boundary, the following momentum and continuity terms are satisfied:

$$\text{continuity} \qquad \int \rho u_j n_j \ \mathrm{dS} \tag{1}$$

$$\text{momentum} \qquad \int \rho u_j u_i n_j \ \mathrm{dS} + \int p^{spec} n_j \ \mathrm{dS} \tag{2}$$

where ρ is the density, u is the velocity component, and n is the normal vector component. Along the sides of the domain either periodic or symmetry boundary conditions are used, depending on the case of interest. For periodic boundary conditions, a master/slave relationship is established between opposite sides of the domain such that enthalpy, momentum, and mass balance are conserved for the opposing nodes as if it were a single node. For symmetry boundary conditions no net mass flux is allowed across the boundary.

Material properties

For isothermal conditions the material properties associated with the model are given in Table 1. Note that the properties for water correspond to an operating temperature of 394.2 K. For the nonisothermal cases, Table 2 gives the values from which relevant properties were extrapolated from.

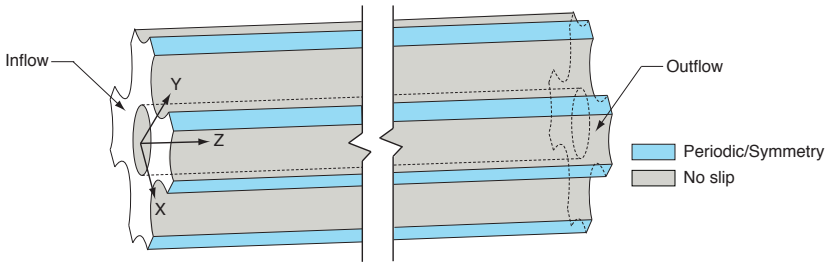

Figure 2: Problem boundary conditions. Although not shown, no slip boundary conditions are also applied to the surface of the spacers and mixing vanes.

Table 1: Isothermal material properties

Parameter	Value
Fluid	Water
Temperature	394.2 K
Viscosity	2.32 $\times 10^{-4}$ $Pa \cdot s$
Density	942.0 kg/m^3

Table 2: Nonisothermal material properties

Temperature (K)	Viscosity ($Pa \cdot s \times 10^{-4}$)	Density (kg/m^3)	Enthalpy (kJ/kg)
298	8.91	997.38	1245.64
363	3.15	965.06	1517.34
422	1.86	918.0	1763.96
589	0.86	678.7	2462.02

Turbulence modeling

Due to the high dependency of the excitation forces on temporally varying fluctuations in the flow field, Large Eddy Simulation (LES) turbulence modeling was used as the closure model for this analysis with the dynamic Smagorinsky subgrid scale model.

Data analysis locations

Several points were selected as planar locations for harvesting data. These points are listed in Table 3. When the recoded data is pointwise, the location is denoted as Location A-x for the point on the surface of the fuel rod at $z = 31.269D$, $x = D/2$, and $y = 0$. These points are also shown in Figure 1. To further clarify the location selected for the trailing edge of the spacer, Figure 3 shows the coordinates of the tip of the trailing edge.

Computational Aspects

Fuego employs a segregated projection method approach to solve the governing equations for mass, momentum, and energy balance. In particular, the projection method calculates a pressure field that is consistent with the velocity field such that continuity is satisfied. Various pressure-smoothing methods are

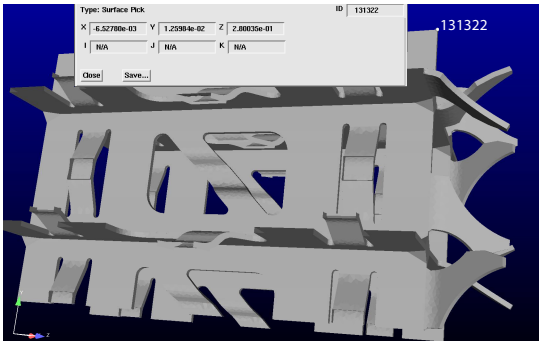

Figure 3: Image showing the location of the trailing edge in the downstream direction of the spacer assembly. The point $z = 0.280035$ corresponds to $29.48D$.

Table 3: Plane locations used for data collection

Point	Location
A	$z = 31.269D^*$
B	$z = 32.953D$
C	$z = 34.744D$
D	$z = 37.257D$
E	$z = 40.011D$

* The diameter of the fuel rod is 0.0095 m.

available to avoid pressure decoupling in the co-located mesh. The selected upwind method interpolates the convected values onto the control volume faces.

Table 4 shows a number of representative values related to the numerical computations. The time step was selected such that a constant CFL number of 2.0 was obtained. As a result, the time step varied during the simulations and for each mesh. Regardless, the time step did not vary much from the value reported in Table 4. Figure 4 shows the cross-section of various meshes and sizes for each mesh are reported in Table 5. Complications due to clusters of elements in the vicinity of sharp corners in the spacer resulted in unusual statistics regarding the number of elements in the mesh and the average sizes. Although several meshes of increasing resolution were run for each simulation, we were unable to obtain uniformly refined sets of meshes. We intend to resolve this issue in forthcoming work.

Table 4: Values used for numerical computations

Parameter	Value
CFL limit	2.0
Time step	$1 \times 10^{-5} s$
Nonlinear residual norm tolerance	1.0×10^{-7}
Solution duration	1.0 s

Fluid-structure Interaction

As part of this work we developed a method for transferring the tractions generated by the CFD results to the fuel rod assembly. Salient features of the proposed method include:

Table 5: Mesh size metrics. The size was computed as the mean of the element area for a slice taken in the $x - y$ plane.

Mesh	Cross-stream Area ($m^2 \times 10^{-8}$)	Max Volume ($m^3 \times 10^{-13}$)	Min Volume ($m^3 \times 10^{-13}$)
3d-10d 664k elem	146.707	30520.4	1.97933
3d-10d 1224k elem	13.8292	1996.41	2.08953
3d-10d 1932k elem	9.39153	1240.69	2.37629
3d-10d 5832k elem	4.35004	363.885	4.11829
full 725k elem	146.645	30557.1	2.08952
full 1450k elem	23.82	4778.38	2.08333
full 2169k elem	60.79*	9497.16	4.19740

* The mean element size for the full 2169k elem mesh is larger than the full 1450k elem mesh (even though it has more elements) due to an issue with the full 2169k elem mesh having an inordinate number of elements clustered around a part of the mixing vane. The cross-stream refinement was actually coarser for this mesh.

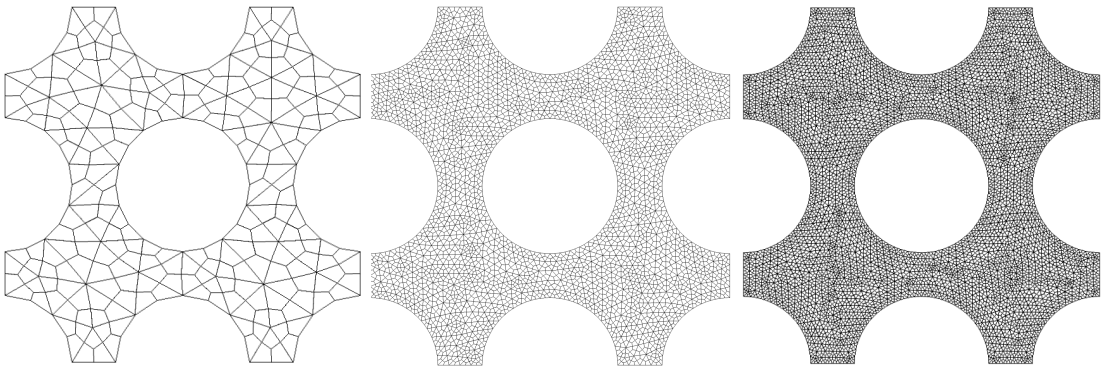

Figure 4: Cross-sections of various meshes (left) 3d-10d 664k elem (middle) 3d-10d 1932k elem (right) 3d-10d 5832k elem.

- Data can be extracted from existing CFD results without the need to re-run simulations
- Any code that produces ExodusII output can be coupled to the vibrational response
- Different resolutions for the fluid and solid mesh can be handled
- Interpolation of time planes is handled automatically
- Multiple means of providing tractions (pressure alone or including shear stress, etc) are accommodated
- The compute times for the fluid or solid analysis is not impacted

One-way coupling of the CFD results to the vibrational analysis is achieved by using the data interpolation tools provided by the Sierra framework. During a pre-processing stage, an ExodusII file is read into memory and nodal data for pressure or external force is interpolated to faces on the solid mesh. When the vibrational response is run in Sierra/Presto an input command line informs the code to read the pressures from these faces.

Fully coupled analysis whereby the motion of the fuel rod in-turn influences the flow is also possible using the Sierra framework and poses an interesting topic to explore in future work.

Results and Discussion

In the following section we present results for a number of simulations related to various aspects of GTRF including analysis of the pressure loading on the fuel rod, the pressure drop across the spacer grid, frequency of the loading, changes due to nonisothermal conditions, and coupled fluid-structure interaction results.

Turbulent pressure fluctuations on the fuel rod surface

Pressure time histories at various locations for several meshes are shown in Figure 5. The locations nearest the spacer gird and mixing vanes exhibit the largest magnitudes and fluctuations as expected. Initial transients take approximately 0.1 seconds to stabilize for each of the meshes. Figure 5 also shows that the pressure dies off quickly as the distance from the mixing vanes increases. As the resolution of the full length meshes approach that of the 3d-10d domain, the pressure solutions approach the same mean values. These two observations suggest that truncating the domain from the full length to the 3d-10d domain is a valid model simplification. The mean and standard deviation of the pressure at Location A-x is shown in Table 6 and Figure 6.

Table 6: Mean and standard deviation of the pressure at location A-x for various meshes. Mesh sizes are reported in Table 5.

Mesh	Mean (kPa)	Std. Deviation (kPa)
3d-10d 664k elem	10.5947	0.60555
3d-10d 1224k elem	2.1475	0.91658
3d-10d 1932k elem	1.6515	0.96414
3d-10d 5832k elem*	3.0191	1.25967
full 725k elem	34.4641	0.62855
full 1450k elem	8.7700	0.26637
full 2169k elem	16.6751	0.87447

* Results for this mesh were obtained using a MUSCL scheme for upwinding rather than the first-order scheme that was used for the rest of the meshes.

The mean pressure drop across the spacer is reported in Table 7 and Figure 7. The pressure drop was computed as the difference between the pressure averaged over the intersection of two planes with the fuel rod surface. The first plane is at $z = 23.41D$ and the second is at $z = 31.27D$.

Table 7: Mean pressure drop across the spacer for various meshes for the 3d-10d domain. Mesh sizes are reported in Table 5.

Mesh	Pressure Drop (kPa)
3d-10d 664k elem	31.85
3d-10d 1224k elem	24.64
3d-10d 1932k elem	24.37

The net driving force in any direction can be calculated by integrating the pressure over a subset of the surface of the fuel rod and taking the dot product of the surface normal with the direction of interest. The mean pressure force in the x-direction is shown in Figure 8. Notice again that the force dies off quickly as the distance from the mixing vane increases. These results roughly match the pressure loading in the x-direction reported by [6].

Periodic boundary conditions

Simulations are currently underway for 3d-10d meshes of resolution 670k, 1000k, 2000k, 5800k, 7200k, and 12500k using periodic boundary conditions along the sides of the domain. At the time of this writing, several of these meshes have reached pseudo-steady-state and the analysis is ongoing.

Frequency of vibrational loading

Fast Fourier transforms of the pressure loading at several locations (shown in Figure 9) reveal that the dominant frequencies of the fluctuations are distributed over a large spectrum from 0 to 5,000 Hz. Experimental results show that a typical frequency of vibration for a fuel rod is on the order of 30 Hz [7]. This suggest that the vibrational response of the fuel rod filters out high frequency pressure fluctuations. The same behavior is exhibited in a subsequent section containing coupled results. The dynamic response of the fuel rod involves vibration at a frequency much closer to the natural frequency of the structure rather than the high frequency pressure fluctuations.

Swirling flow

A critical aspect of the flow of coolant though the reactor involves swirling induced by the mixing vanes. This type of mixing can be seen in Figure 10 which shows vector plots of the in-plane velocity for two locations in the 3d-10d domain. The results in Figure 10 were produced by averaging the velocity over a window of time beginning after the initial transient stage. Notice that for the plane nearest the mixing vane (Location A) the vortical structure that forms is similar to the PIV data reported by [8] and the magnitude of the flow is similar to the simulated results presented. These results also compare nicely with those reported in [6]. For the planes taken near the outflow boundary, the swirling structure of the flow is clearly identified. As expected, the finer mesh better resolves the vortical structures outside of the main swirling vortex.

Nonisothermal conditions

To evaluate the degree to which heat transfer affects the results additional simulations were run under nonisothermal conditions. Although a more realistic scenario would include a sinusoidal temperature profile, for this set of results, the fuel rod surfaces were held at a constant temperature of 500 K while the coolant was injected at 394.2 K. A snapshot in time of the temperature is shown in Figure 11 which shows that the heat transfer is considerably affected by the swirling flow created by the mixing vanes as intended. Figure 12 shows that the vortex structure in the subchannels is relatively the same for the isothermal and nonisothermal cases.

Coupled fluid-structure interaction results

As a prototypical example, in this section we demonstrate the coupling method discussed above for a simplified version of the full fuel rod model presented in [9]. Unlike the complex solid model that contains pellets, gaps, springs, and dimples, the simplified model involves a simply-supported solid cylinder with the properties defined in Table 8. Results generated by both Fuego and Drekar (presented in [10]) were used to excite the solid cylinder. Figure 13 shows the displacement of the centroid of the cylinder in time as it is loaded by the fluid pressure. A fast Fourier transform of the displacement is shown in Figure 14. Although all

Table 8: Solid cylinder properties.

Property	Value
Length, L	0.528028 m
Diameter, D	0.0095 m
Young's Modulus, E	$6.8887\times10^{10} Pa$
Poisson's Ratio, ν	0.342
Density, ρ_s	10900 kg/m^3

cases excite the same mode of vibration (similar frequency) the nonisothermal forcing induces much higher amplitudes. The source of this phenomena should be investigate in future work.

The natural frequency of vibration, f_n, for this cylinder can be computed as 33.63 Hz from the following equation:

$$f_n = \frac{k}{2\pi L^2}\text{sqrt}(EI/m) \tag{3}$$

where $k = 9.87$ is a constant related to the first mode of vibration, m is the mass per unit length, and I is the area moment of inertia. The computed frequency of vibration for the simulation is 35.16 Hz in both the x and y-directions. The coupled results should not match the free vibration natural frequency exactly because the vibration is influenced by the surrounding fluid, but the frequencies should not differ greatly. The initial transients shown for the Fuego result are due to the fact that the Drekar results were truncated to exclude the initial transients.

Summary

We have presented results for a number of Fuego simulations related to GTRF. The isothermal, fluid-alone calculations show that the truncated domain is suitable for this analysis. They also show strong correlation with other published results for the pressure load along the fuel rod and structure of the flow within the subchannels. The nonisothermal simulations show that most of the heat exchange happens downstream of the grid spacer as expected and produces higher amplitude vibrations when coupled with the solid model. Lastly, the coupled results suggest that the method for interpolating the pressure loads from the CFD calculations to the structural mesh works well for incorporating Fuego results as well as results from other codes.

This work highlights a number of areas ripe for further investigation including: better mesh refinement strategies (particularly in the spacer region) and corresponding verification studies, more detailed analysis of the role of heat transfer and its relationship to the structural vibrations, and more extensive comparison of various turbulence models. These studies will provide much higher fidelity models for analyzing GTRF related problems.

Appendix

Figures 15 and 16 show selected validation results for swirling jets and swirling jets in crossflow which are key flow phenomena present inside nuclear reactors. Other validation and verification results are available upon request.

Acknowledgments

The authors would like to thank Stefan Domino for his work on getting several of the examples up and running and providing frequent consultation. The authors would also like to thank Rick Garcia for generating the meshes as well as the Drekar team (John Shadid, Tom Smith, and Roger Pawlowski) and Bill Rider for fruitful discussions regarding the results. Lastly, we thank Alan Williams and Sam Subia for help with the Sierra framework, Robert Baca for user support, and the Westinghouse engineers (Zeses Karoutas, Roger Lu, and Abdel Mandour) for generously providing geometries and results for comparison.

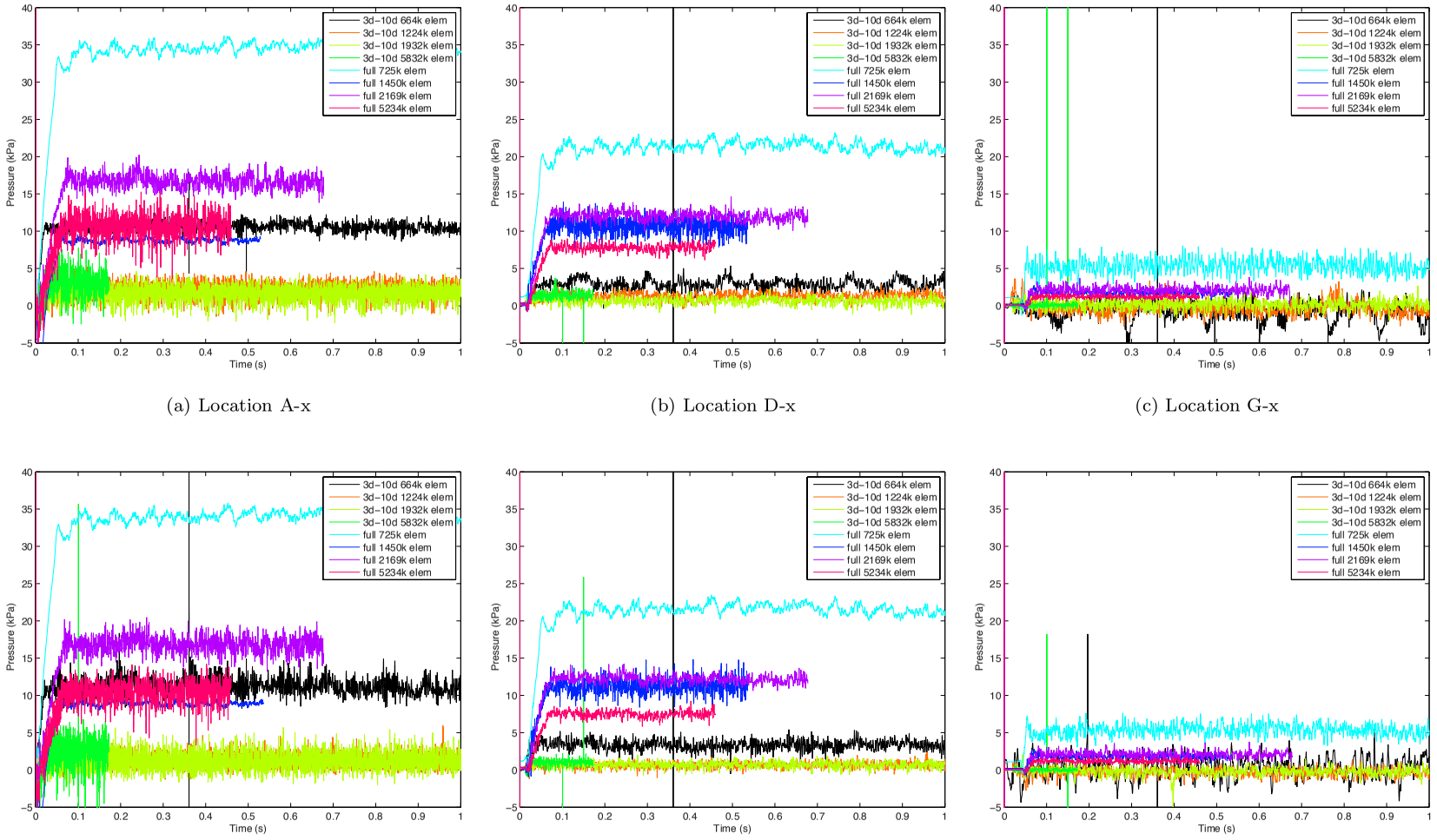

(a) Location A-x

(b) Location D-x

(c) Location G-x

(d) Location A-y

(e) Location D-y

(f) Location G-y

Figure 5: Pressure time history at various locations for various meshes.

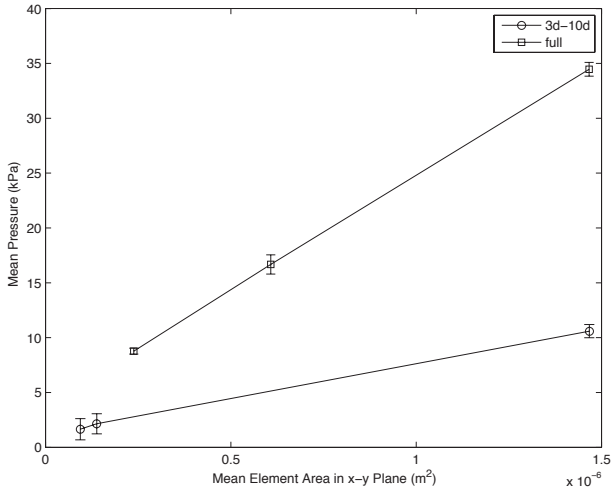

Figure 6: Mean pressure values for location A-x for various mesh sizes. The mean pressure was computed as the average over the time window (0.08,1.0) seconds. The element area was computed for a slice taken in the $x - y$ plane. Results are reported for both the full length domain and the 3d-10d domain in Table 6.

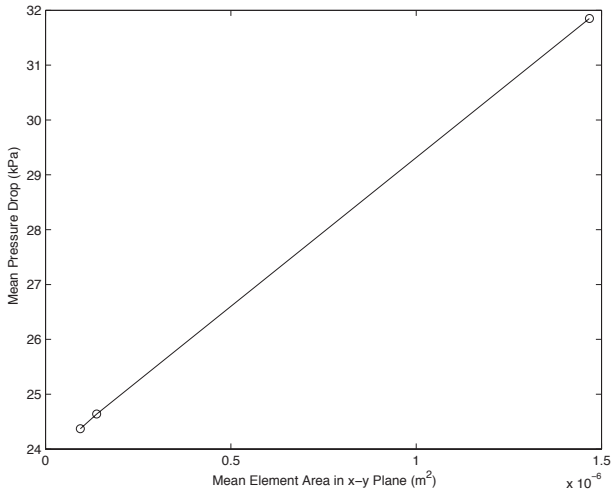

Figure 7: Pressure drop across the spacer for various mesh sizes for the 3d-10d domain. The element area was computed for a slice taken in the $x - y$ plane.

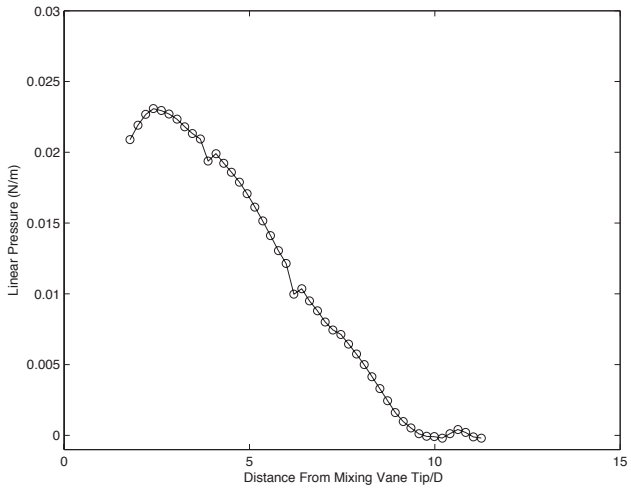

Figure 8: Mean value of the pressure force in the x-direction vs. distance from the mixing vane tip for the 3d-10 1932k elem mesh computed as the integral of pressure over a sub-surface of the fuel rod surface divided by the length of the sub-surface.

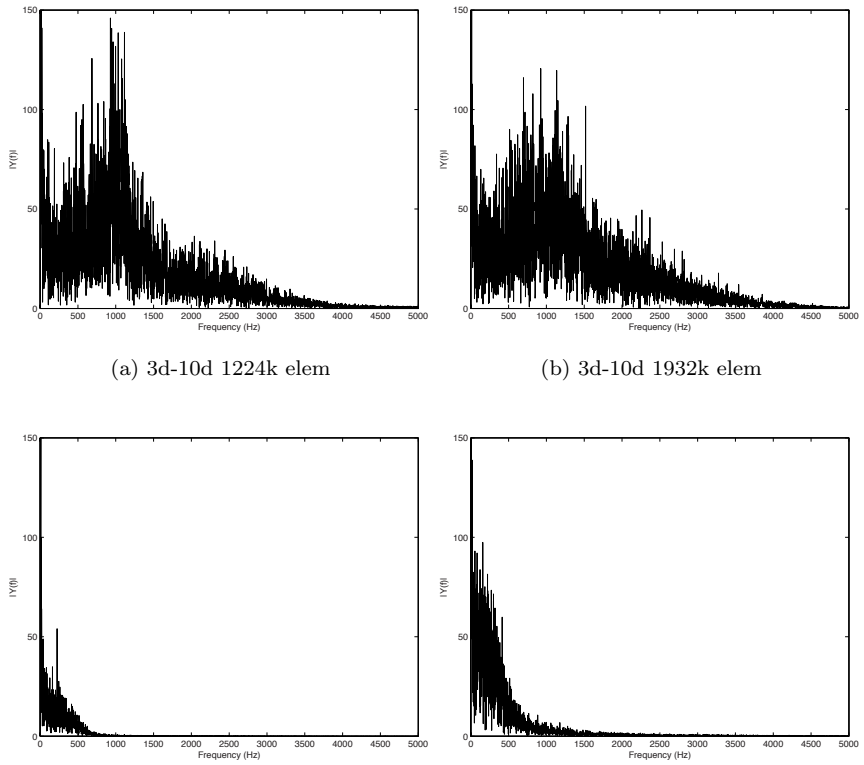

(a) 3d-10d 1224k elem

(b) 3d-10d 1932k elem

(c) full 1450k elem

(d) full 2169k elem

Figure 9: Fast Fourier transforms of the pressure time history at location A-x for various meshes.

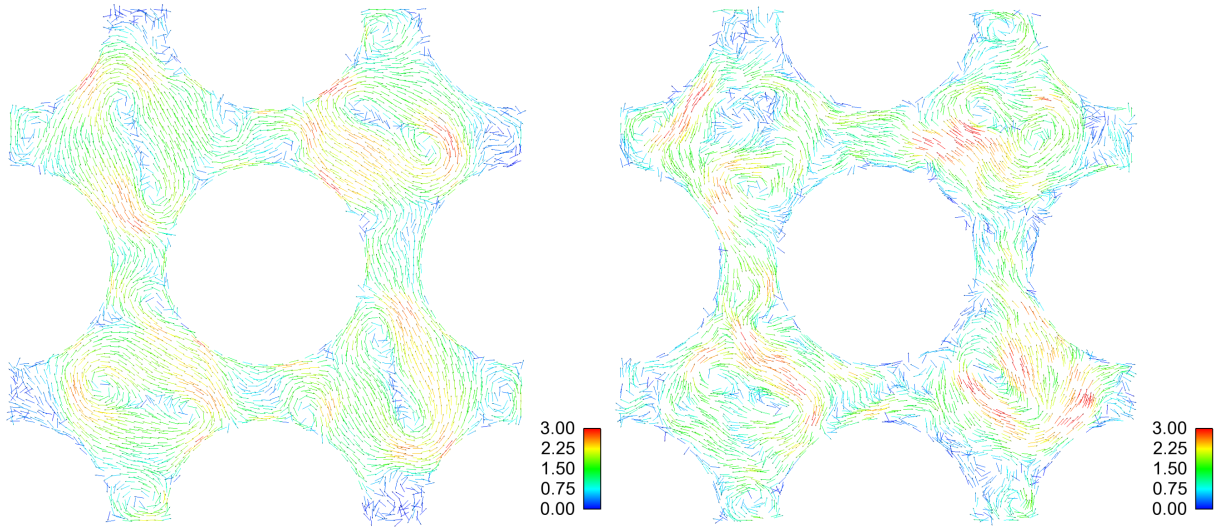

(a) Location A 3d-10d 1932k elem

(b) Location A 3d-10d 5832k elem

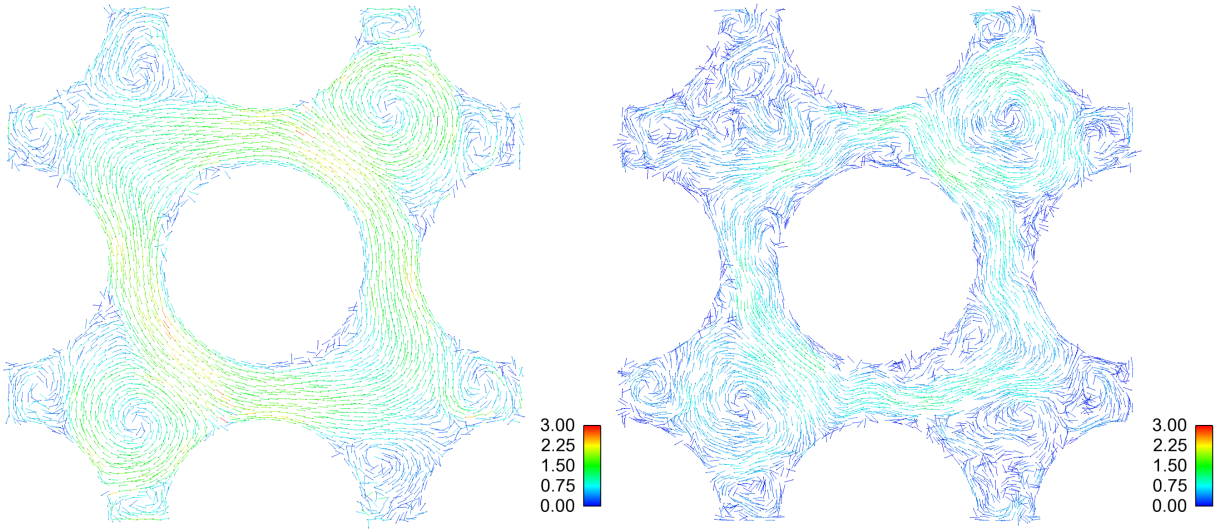

(c) Location E 3d-10d 1932k elem

(d) Location E 3d-10d 5832k elem

Figure 10: Average x-y velocity magnitude vectors (m/s) for the 3d-10d 1932k elem and 3d-10d 5832k elem mesh at locations A and E. Only the x and y components of the velocity are included in the magnitude.

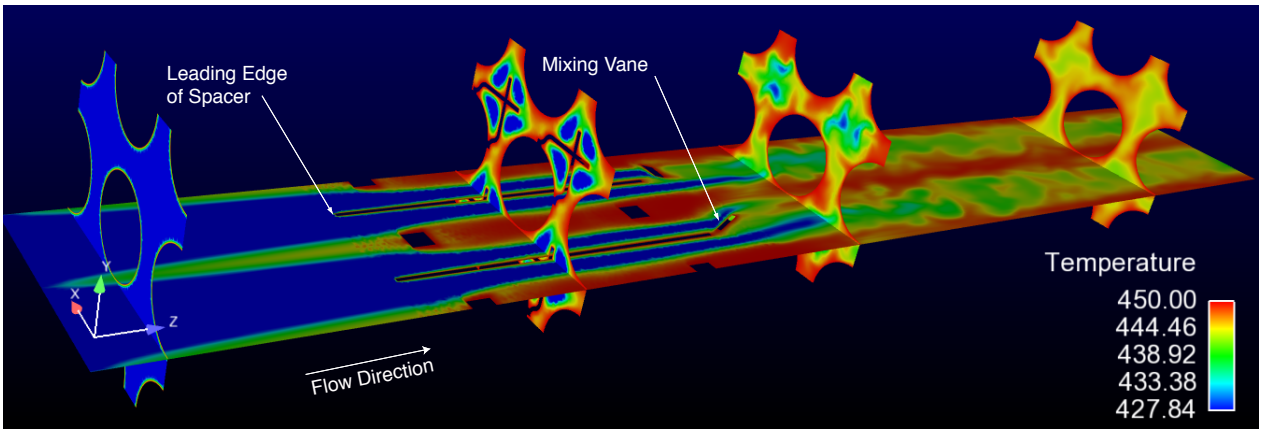

Figure 11: Contours of temperature (K) for the 3d-10d 5862k elem mesh at time $t = 0.02s$. Note the improved heat exchange downstream of the mixing vanes.

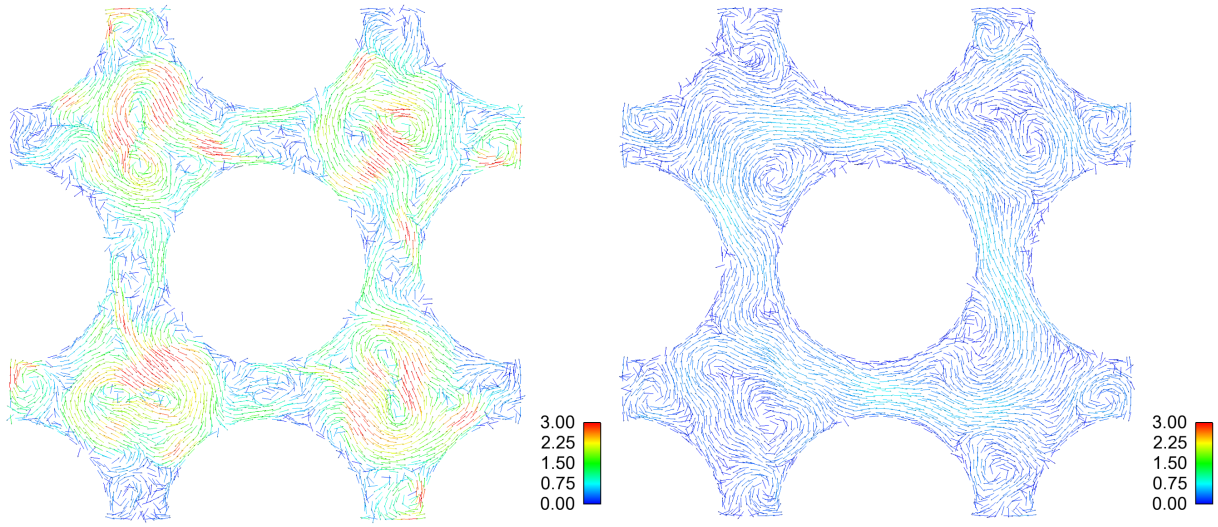

(a) Location A

(b) Location E

Figure 12: Average x-y velocity magnitude vectors (m/s) for the nonisothermal 3d-10d 5832k elem mesh at locations A and E. Only the x and y components of the velocity are included in the magnitude.

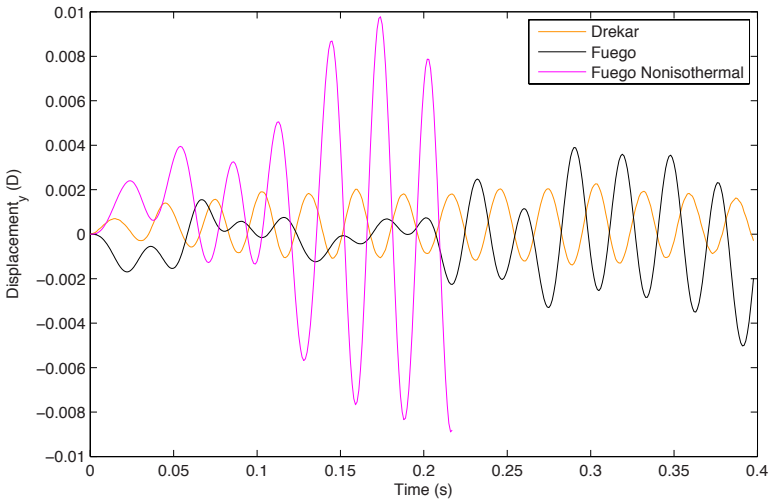

Figure 13: Displacement in the y-direction produced by the fluid loads in time.

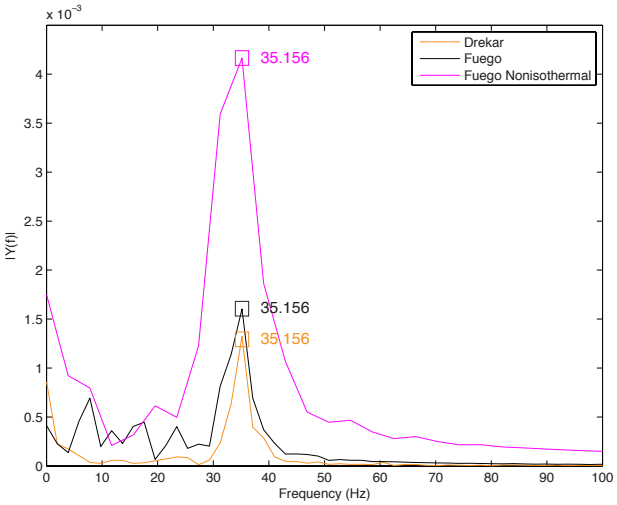

Figure 14: Fast Fourier transform of the displacement in the y-direction.

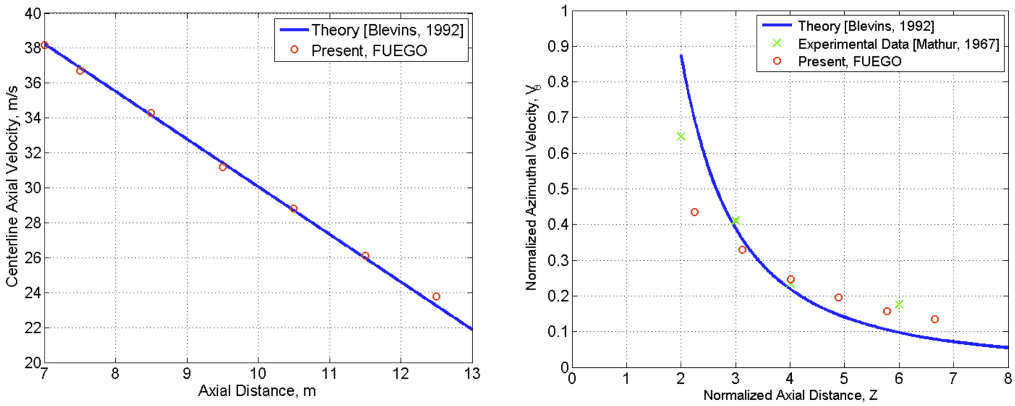

Figure 15: Swirling jet: (left) axial and (right) azimuthal velocity vs. axial distance

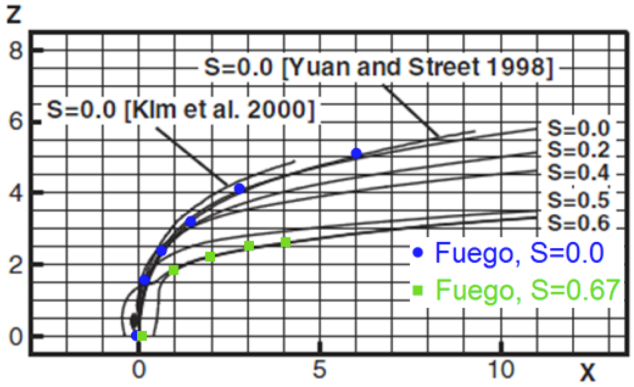

Figure 16: Swirling jet in cross-flow: comparison of various LES simulations

References

[1] Fuego. SIERRA/Fuego 2.7 User's Manual. *Sandia National Laboratories*, SAND 2006-6084P, 2008.

[2] S. B. Rodriguez and M. S. El-Genk. Numerical investigation of potential elimination of "hot streaking" and stratification in the VHTR lower plenum using helicoid inserts. *Nuclear Engineering and Design Journal*, 240:995–1004, 2010.

[3] S. B. Rodriguez and M. S. El-Genk. Cooling of an isothermal plate using triangular array of swirling air jets. *14th International Heat Transfer Conference, Washington DC*, 2010.

[4] S. B. Rodriguez, S. Domino, and M. S. El-Genk. Safety analysis for the NGNP lower plenum using the Fuego CFD code. *CFD4NRS-3 Workshop, Experimental Validation and Application of CFD and CMFD Codes to Nuclear Reactor Safety Issues, Washingon, DC*, September 14-16, 2010.

[5] J. Wan. Westinghouse Electric Company Memo. *Subject: V5H Fuel Assembly CAD Model and CFD Model Transmittal*, December 10, 2010.

[6] S. Benhamadouche, P. Moussou, and C. Le Maitre. CFD estimation of the flow-induced vibrations of a fuel rod downstream a mixing grid. *Proceedings of the ASME 2009 Pressure Vessels and Piping Division Conference*, PVP2009-78054, July, 2009.

[7] R. Y. Lu. Westinghouse Electric Company Memo. *Subject: 17x17 V5H VIPER Test and Instrumented Fuel Rod General Mechanical Information Transmittal to CASL Project, Non-proprietary*, April 13, 2011.

[8] A. M. Elmahdi, R. L. Lu, M. E. Connor, Z. Karoutas, and E. Baglietto. Flow induced vibration forces on a fuel rod by LES CFD analysis. *In Review: The 14th International Topical Meeting on Nuclear Reactor Thermal Hydraulics (NURETH-14), Ontario Canada*, September 25-29, 2011.

[9] N. K. Crane *et. al.* Analysis integration procedures for Grid-to-Rod Fretting (GTRF) test problem. *Sandia National Laboratories*, 2011.

[10] J. N. Shadid *et. al.* Initial Drekar LES CFD simulations for Grid-to-Rod Fretting (GTRF). *Sandia National Laboratories*, 2011.

DISTRIBUTION:

1	MS 0836	Ryan Bond, 1541
1	MS 0899	RIM-Reports Management, 9532 (electronic copy)

Sandia National Laboratories